Journal of Quantitative Spectroscopy & Radiative Transfer 119 (2013) 53–66

Contents lists available at SciVerse ScienceDirect

Journal of Quantitative Spectroscopy & Radiative Transfer

journal homepage: www.elsevier.com/locate/jqsrt

Impact of morphological parameters onto simulated light scattering patterns

Krzysztof Skorupski [a,b,*], Janusz Mroczka [a], Norbert Riefler [b], Hergen Oltmann [c], Stefan Will [d], Thomas Wriedt [e]

[a] Wroclaw University of Technology, Chair of Electronic and Photonic Metrology, Boleslawa Prusa 53/55, 50-317 Wroclaw, Poland
[b] Universität Bremen, MVT, Badgasteiner Str. 3, 28359 Bremen, Germany
[c] Universität Bremen, Technische Thermodynamik, Badgasteiner Str. 1, 28359 Bremen, Germany
[d] Universität Erlangen-Nürnberg, Lehrstuhl für Technische Thermodynamik, Am Weichselgarten 8, 91058 Erlangen, Germany
[e] Institut für Werkstofftechnik, Badgasteiner Str. 3, 28359 Bremen, Germany

ARTICLE INFO

Article history:
Received 21 August 2012
Received in revised form
7 December 2012
Accepted 12 December 2012
Available online 31 December 2012

Keywords:
Fractal aggregates
Light scattering
T-Matrix
DDScat

ABSTRACT

We have investigated the impact of the variation of various parameters of fractal aggregates on simulated light scattering patterns. Static light scattering is commonly used to measure soot in a flame and such a study could help to improve experimental approaches. Aggregate models, used for our light scattering simulations, are based on real soot structures that can be found under laboratory conditions in a premixed ethane/air flame (McKenna-type burner, equivalence ratio $\phi = 2.5$). Our work was not focused on modeling and analysis of aggregates that are typically encountered in the atmosphere, therefore the results might be of limited interest to climate scientists. In our study, the variation of all parameters that enter into the standard fractal equation were investigated. Additionally effects when varying the overlap of primary particles, the incident wavelength and the complex refractive index are discussed. For numerical simulations two different codes were used, the T-Matrix (when particles are in point contact) and the DDScat program (which is capable of performing light scattering simulations by overlapping spheres). Comparisons between these two methods show very good agreement. The results demonstrate that the radius of gyration is responsible for the amount of light scattered towards the back direction while the total volume of an aggregate defines the shape of the light scattering patterns. Small changes of the fractal dimension can be neglected (provided that the fractal prefactor is accordingly modified in a suitable way). The overlap level, if the radius of gyration is kept constant, introduces barely visible changes to the light scattering diagrams which suggest that a simple aggregate model, composed of particles being in point contact, can be used instead of a structure in early sintering stage when overlap of primary particles is not so high.

1. Introduction

Soot aggregates are products of incomplete combustion of organic fuels and are composed of a few, up to several hundred almost spherically shaped primary particles. Their morphology parameters are dependent on the individual combustion process, fuel composition, flame type and other technical aspects. Many techniques for determination of the morphology of soot aggregates have been developed. One of the most important techniques is

* Corresponding author at: Wroclaw University of Technology, Chair of Electronic and Photonic Metrology, Boleslawa Prusa 53/55, 50-317 Wroclaw, Poland. Tel.: +48 71 320 63 09.
E-mail addresses: krzysztof.skorupski@pwr.wroc.pl (K. Skorupski), janusz.mroczka@pwr.wroc.pl (J. Mroczka), riefler@iwt.uni-bremen.de (N. Riefler), hergen.oltmann@uni-bremen.de (H. Oltmann), sec@ltt.uni-erlangen.de (S. Will), thw@iwt.uni-bremen.de (T. Wriedt).

0022-4073/$ - see front matter © 2013 Elsevier Ltd. All rights reserved.
http://dx.doi.org/10.1016/j.jqsrt.2012.12.014

TEM (transmission electron microscopy) analysis. However, it provides us with 2D projections of 3D fractal-like structures only. The lack of one dimension results in many difficulties and noticeable errors that persist in every method commonly used to derive morphological parameters from such images (e.g. [1,2]). Moreover, online-measurements are impossible to perform and the sampling process is considered to be quite invasive [3,4]. To overcome some of these problems, a new technique called ET (electron tomography) was created [5,6]. It is strictly associated with the TEM approach. A series of 2D images, collected from different viewing angles, are combined into representations which are capable of displaying morphological parameters of 3D structures. Because there is no simple formula for deriving 3D parameters from 2D images (e.g. the fractal dimension D_f), ET is considered to be much more accurate technique than TEM [5]. Optically based techniques, e.g. LII (laser-induced incandescence) [7–9] and ELS (elastic light scattering) [10] are capable of performing on-line measurements. The first one can be used to measure the size of primary particles and the second one to determine the fractal dimension as well as the soot volume fraction of aggregates. A new experimental approach, WALS (wide-angle light scattering), is capable of performing fast on-line measurements with a high angular resolution in the scattering pattern [11,12].

To model the light scattering by fractal-like structures many theories and programs have been developed so far. One of the most important is the Null-Field theory (also known as T-Matrix theory), proposed by Waterman [13], which is considered as numerically exact in its current implementation. However, it is limited to a single particle and cannot be used for more complex structures. For a more general treatment, the superposition T-Matrix method (capable of performing light scattering simulations by aggregates composed of particles being in point contact) has been developed. Another valuable theory is DDA (discrete dipole approximation), which was proposed by DeVoe [14,15] and improved by Purcell and Pennypacker [16]. It can overcome the point contact limitation. However, the computation time is significantly higher.

The main goal of this paper is to create a set of model aggregates similar to real soot structures, as inferred by TEM, and to investigate the impact of the standard fractal equation parameters and additionally the effect of the refractive index, the incident wavelength and the overlap between particles on the resulting light scattering diagrams. The aggregate model is based on the TEM analysis of 110 soot structures and the morphological parameters were calculated using the method proposed by Brasil et al. [1].

This study can help to develop effective soot characterization methods based on measuring static light scattering. We will first compare the T-Matrix program of Doicu et al. [17] with the DDScat program, written by Draine et al. [18] to show that both theories are capable of performing reliable light scattering simulations and provide us with almost identical light scattering results. Secondly, we create a soot aggregate model which is based on TEM analysis. The light scattering results by our model are compared to WALS measurements. Finally, we determine the impact of the variation of its parameters on the light scattering patterns.

2. Theoretical background

Soot aggregates are mostly described as fractal-like structures which are characterized by parameters which are considered to remain constant during the whole aggregation process. Fractal aggregates can be described by the equation:

$$N_p = k_f \left(\frac{R_g}{r_p}\right)^{D_f}, \tag{1}$$

where N_p is the number of primary particles, r_p is the particle radius and R_g denotes the radius of gyration of the structure. The fractal behavior is defined by two factors—the fractal dimension D_f and the fractal prefactor k_f. It was proven that the first one is independent of the size of the structure [19] and for freshly emitted particles its value is usually considered as $D_f \approx 1.8$ [20,21] what is typical for DLCA (diffusion limited cluster aggregation) process [10]. By the contrary, recent study (by the use of electron tomography measurements) suggests that this value might be underestimated and should be assumed as $D_f = 2.4$ [20]. Moreover, due to the aging effect soot aggregates may collapse and form more compact clusters [22,20] with the fractal dimension even as high as $D_f = 2.6$ [23]. The pseudo-fractal behavior of an aggregate cannot be described by a single parameter, also the fractal prefactor k_f is needed. Its origins and behavior are yet not fully clear. Moreover, its value changes from almost 1 to 3.4 according to various publications [24] and is dependant on the experimental set-up as well as on environmental conditions [21]. The radius of gyration can be expressed by the following equation:

$$R_g^2 = \frac{1}{N_p}\sum_{i=1}^{N_p}(r_i - r_0)^2, \tag{2}$$

in which r defines the position of a single particle in the structure and r_0 the geometrical center of the cluster. However, this is not the only suitable formula. For example Filippov et al. suggest the following correction [25]:

$$R_g^2 = \frac{1}{N_p}\sum_{i=1}^{N_p}(r_i - r_0)^2 + r_p^2. \tag{3}$$

They assume that the radius of gyration should also include all points on the spherule surfaces instead of the mean square of the distance between particles and the mass center. The resulting difference is only visible for aggregates that consist of very few spheres. In contrast, the overlap factor, defined by the equation:

$$C = 1 - \frac{l}{2r_p} = 1 - \frac{l}{d_p}, \tag{4}$$

where l defines the distance between centers of two particles, has an undeniable impact on the fractal prefactor [1]. It also affects the fractal dimension, but this change is less significant [26,27].

Soot particles are usually considered as non-overlapping spheres being only in point contact. Such approach has many advantages (e.g. can significantly decrease the computational

time). However, it does not represent the real structures as seen from TEM images. The overlap factor exists, recent experimental observations in various types of flames found a value of $C \approx 0.25$ according to Oltmann et al. [11]. The changes to the fractal morphology, caused by the overlap factor, can be expressed as follows [27]:

$$k_f = 1.3e^{2.2C}, \tag{5}$$

$$R_g = R_{g_0}(1-C), \tag{6}$$

where R_{g_0} refers to the initial radius of gyration of the aggregate (assuming $C=0$) and the value of 1.3 is assumed to be the initial fractal prefactor.

3. Comparison of the light scattering programs

To demonstrate that the DDScat program is capable of simulating light scattering by touching as well as overlapping spheres, a sample soot model, based on the aggregation method proposed by Filippov et al. [25], was created ($C=0.00$, $N_p=100$, $D_f=1.78$, $k_f=1.50$, $r_p=10.00$ nm and $R_g=105.37$ nm). However, in the literature, many alternative methods for generating aggregates can be found, e.g. [28,29]. In nature, particles always overlap ($C>0$). The simplification ($C=0$) is due to the T-Matrix code, which is not capable of simulating the light scattering phenomena of overlapping spheres. Both the T-Matrix and DDScat code were used to compute scattering diagrams. The wavelength was $\lambda = 514.5$ nm and the value of the refractive index was taken as $m = 1.57 + 0.56i$. For the DDScat simulations the whole structure was divided into $N_d=6553$ volume elements (dipoles) what resulted in a discretization of approximately 128 points per wavelength. The DDScat criterion, described by

$$|m|kd < 1, \tag{7}$$

was obviously met ($|m|kd \approx 0.081$). In this formula m stands for the complex refractive index, d is the distance between dipoles in the resulting mesh and $k = 2\pi/\lambda$ is the wave number, where λ represents the chosen wavelength in vacuum. The T-Matrix approach, considered as exact, was taken as the reference. The resulting, normalized scattering diagrams are shown in Fig. 1. However, due to the huge similarity between both programs the difference is difficult to observe. Fig. 2 presents the relative error of the DDScat results, which is expressed by

$$E_{Rel}(\theta) = \frac{X(\theta) - Ref(\theta)}{Ref(\theta)} \cdot 100\%, \tag{8}$$

where θ is the scattering angle. The averaged error, which covers deviations in many orders of magnitude, is defined as

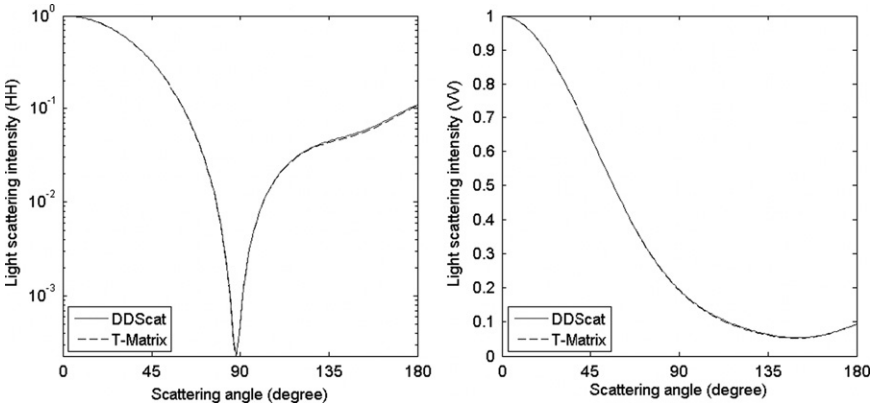

Fig. 1. Comparison of the T-Matrix with the DDScat program. Normalized results of both simulations are presented.

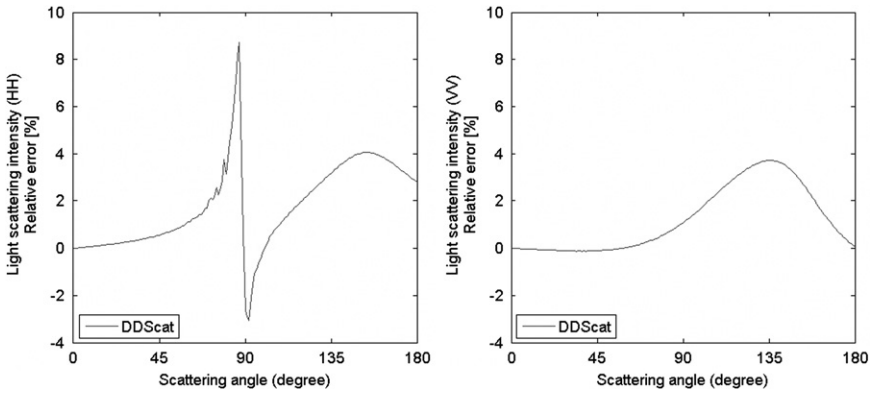

Fig. 2. Comparison of the T-Matrix with the DDScat program. Relative errors of both simulations are presented.

follows:

$$E_{Avg}[\%] = \frac{\sum_{\theta=0}^{n} |E_{Rel}(\theta)|}{n}. \quad (9)$$

The term "error" can be misleading because the exact values remain unknown. In this paper we assume that the reference data is accurate. However, this is not the exact solution.

The results show that the maximum relative error between the two programs is about 8.72% ($\theta = 87^\circ$) for horizontal polarization and 3.70% ($\theta = 137^\circ$) for vertical polarization. The value of the first error was expected due to the minimum of the scattering pattern localized near the angle of 90°. At this angle the intensity of the scattered light is close to zero. Thus, even a very small change between both approaches can artificially increase the resulting error. Nevertheless, the scattering diagrams show nearly perfect agreement. In each section of this paper either the DDScat (for overlapping particles) or the T-Matrix (when $C < 0.02$) code is used. Detailed discussions concerning the comparison between different light scattering programs can be found elsewhere [30,31].

4. Measured reference data

A reference set of aggregates was used for these investigations and comparisons with the scattering results. The scattering measurements were conducted at the height of 17 mm above a McKenna-type burner (17 mm height above burner, HAB). During the scattering measurements, the total flow of the ethene/air mixture (characterized by the equivalence ratio $\phi = 2.5$) was set to 10 normal liters per minute (NLPM), defined at a pressure of 1013.25 hPa and a temperature of 0 °C. The laser wavelength was $\lambda = 532$ nm. The morphological parameters, resulting from the analysis of 110 TEM images, are presented in Table 1. To emphasize changes caused by the studied parameters, all calculations were based only on averaged data (arithmetic mean) instead of a real distribution. Otherwise results would suffer from additional errors caused by the averaging of light scattering diagrams by very different structures (the number of particles varies from 5 to 149). Note that the averaged data is not based on a log-normal fit, as it was presented in the paper by Oltmann et al. [11]. For this reason, our values are slightly different than in their work. For creating aggregate models a program, based on the algorithm by Filippov (particle-cluster aggregation) [25], was created. The generation of sintered aggregates is a much more difficult and complicated process. However, during early sintering stages this phenomenon can be approximated by a partial overlap between particles [32]. Note that the sintering process is not treated in this paper, the conditions concerning conservation of volume and minimalization of the free energy are not met. Only the influence of overlap level on the resulting light scattering is considered, excluding all other physical and chemical effects. The overlap factor may be implemented in different ways but Eq. (5) must always hold. In the formula, introduced by Brasil et al. [27], the value of 1.3 is assumed to be the initial fractal prefactor for aggregates composed of particles being in point contact. For a more general treatment a variable k_{f_0} is used which stands for the initial fractal prefactor of the structure and should be calculated before initiating the aggregation process:

$$k_{f_0} \approx \frac{e^{2.2 \cdot C}}{k_f}. \quad (10)$$

The k_f parameter refers to the desired fractal prefactor. The radius of gyration should also be adapted. Its change is described by the following formula, which is based on Eq. (6)

$$R_{g_0} \approx \frac{R_g}{1-C}, \quad (11)$$

where R_g is the final (desired) value of the radius of gyration. If we swap the two mentioned parameters and allow particles to overlap during the aggregation process (this procedure leads to decreased value of the radius of gyration), the resulting structure will meet the standard fractal equation in a satisfying way. The fractal dimension is also affected [27,26]. However, in our work it is considered as constant. Because deviation of the overlap parameter tends to zero (barely noticeable fluctuations

Table 1
The averaged values of the TEM measurements and morphology parameters of aggregates included in the reference set.

Type of data	C	N_p	D_f	k_f	r_p (nm)	R_g (nm)
TEM Avg	0.25	33.49	1.78	2.50	9.94	37.65
Simulations	0.00	33.00	1.78	1.84	9.94	50.20

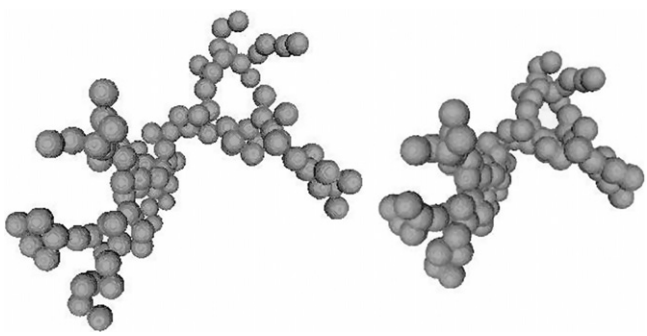

Fig. 3. An aggregate model composed of particles in point contact (left, $C=0$) compared to an aggregate composed of overlapping particles (right, $C=0.25$).

persist) and the overlap level between particles is considered as constant, each particle can be characterized by a similar volume. A sample aggregate model composed of particles in point contact compared to an aggregate that consists of overlapping particles is presented in Fig. 3.

The new morphology parameters (for $C \approx 0$) are presented in Table 1. After generating the reference data set (1000 aggregates) and performing the light scattering simulations using the DDScat code, resulting diagrams were compared to the diagrams obtained by the WALS (wide-angle light scattering) measurements. A detailed description of the experimental set-up as well as the measurement procedure can be found elsewhere [11,12]. The resulting charts for aggregates made of overlapping (curve: TEM Avg) as well as non-overlapping (curve: Simulations) particles in comparison to the measurement data (curve: WALS) are presented in Fig. 4.

The diagram of light scattered by aggregates (for vertical polarization), composed of spheres being in point-contact, is in very good agreement with the WALS measurements. The neglection of the overlap parameter allowed us to create aggregates which give similar light scattering results to real structures. In this case, distributions of the morphological parameters can be neglected completely. This approach may be valid only for fractal-like soot aggregates generated under laboratory conditions discussed in this paper and should not be considered as an universal rule. In the experimental data the characteristic minimum in the diagram for horizontal polarization might be caused by the limited dynamic range of the detection system. However, is also possible that depolarization and cross-polarization is not negligible around the angle $\phi = 90^\circ$ for HH-scattering [10].

5. Results of parameter variations

Every set of aggregates, used to determine the impact of the studied parameters on light scattering diagrams, is composed of a different number of structures (from 1000 to 5000). To generate more accurate light scattering diagrams, configurational averaging was used instead of orientational averaging [33]. However, in many cases a set made up of 1000 aggregates turned out to be not large enough to provide reliable light scattering data. A significant difference in light scattering patterns between sets, composed of aggregates with the same morphological parameters, was observed. During more sensitive study (e.g. the variation of the fractal dimension) this change had a huge impact on the results (and thus on the conclusions). In such a case only if two independent light scattering simulations by different sets (with the same morphological parameters) gave almost identical results,

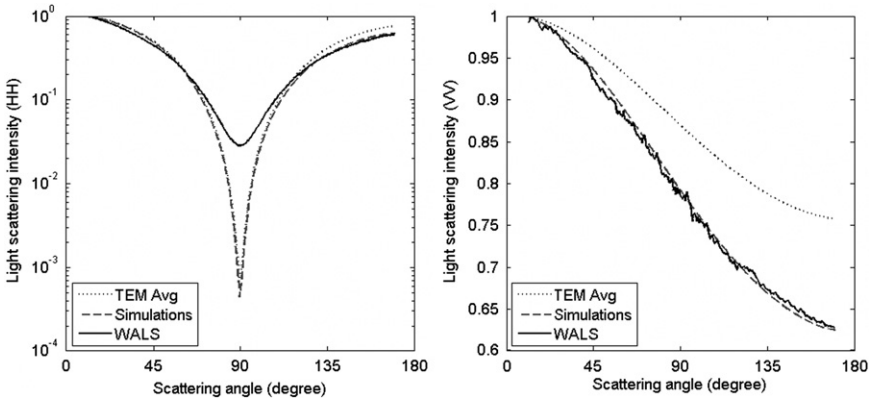

Fig. 4. Comparison of light scattering diagrams obtained by aggregates characterized by different morphology. The curve "Simulations" is related to the aggregate model created for our studies, which is composed of particles in point contact ($C \approx 0$). The curve "TEM Avg" represents the averaged TEM data ($C \approx 0.25$) and the curve "WALS" denotes the measurements.

Table 2
Impact of the number of particles on the light scattering diagrams. Results of the light scattering simulations and parameters of every set of aggregates. Constant parameters: $R_g = 50.20$ nm, $r_p = 9.94$ nm, $D_f = 1.78$.

Set	1	2	3	4	REF	5	6	7	8
N_p (%)	60	70	80	90	100	110	120	130	140
N_p	20	23	26	30	33	36	40	43	46
k_f	1.12	1.29	1.45	1.68	1.84	2.01	2.16	2.41	2.57
C	~0	~0	~0	~0	~0	0.002	0.005	0.007	0.010
Q_{abs}	0.360	0.378	0.395	0.415	0.430	0.444	0.461	0.471	0.484
Q_{sca}	0.005	0.006	0.007	0.009	0.010	0.011	0.013	0.014	0.015
g	0.099	0.097	0.096	0.098	0.098	0.098	0.098	0.100	0.099
MAC (m^2/g)	5.560	5.572	5.589	5.599	5.620	5.637	5.650	5.636	5.662
$E_{Avg/VV}$ (%)	1.952	1.153	0.828	0.431	–	0.053	0.152	0.467	0.162
$E_{Avg/HH}$ (%)	3.487	2.667	1.678	0.924	–	0.417	0.584	1.065	0.974

their size was accepted for further research. Nevertheless, even large (finite) sets should be considered as erroneous.

During our study we discuss the impact of the selected parameter on the light scattering patterns. However, it is not possible to vary only one parameter, because the fractal equation criterion, Eq. (1), must be always met. To describe fractal properties of soot aggregates, two parameters are needed. The fractal dimension D_f and the fractal prefactor k_f. The first one of them is considered to be more influential. For this reason we decided to use k_f as the second variable, which is altered simultaneously with the studied parameter in every step of our study.

5.1. The impact of the number of particles on light scattering diagrams

To check whether the number of particles N_p has a direct effect on the light scattering data, nine different sets of aggregates were created. During this research the deviation of light scattering results, by small sets with the same size (1000 aggregates), was significant. To minimize the resulting error larger sets (5000 aggregates) were used instead. The morphology parameters are listed in Table 2.

For high values of the fractal prefactor ($k_f > 2$) a relatively small overlap error persists ($C \neq 0$). At the beginning of the aggregation process it is not possible to place a new particle in a way that it is only in point contact with the rest of the aggregate. However, due to the existence of this error, the values of the total volume and surface drift away from the expected level (e.g. for an aggregate composed of 46 particles the expected value of $V_A = 189\,237\ \mathrm{nm}^3$ changes to $V_A = 188\,353\ \mathrm{nm}^3$). In our study (Table 2), the overlap error increases along with the number of particles because of the significant (and influential) changes to the fractal prefactor k_f (the overlap level between the first few spheres is larger). A value denoted by ~ 0 means that the overlap error is smaller than E^{-4}, it has minor impact on the results and its influence can be neglected.

For scattering simulations, the T-Matrix program was used. Although this code is considered as not being capable of performing light scattering simulations by sintered aggregates, it turned out that for a small overlap (i.e. $C < 0.015$) the light scattering diagrams, obtained with the use of the DDScat and the T-Matrix program, are almost identical. The resulting errors, $E_{Avg/VV} = 0.15\%$ (for the vertical polarization) and $E_{Avg/HH} = 0.58\%$ (for the horizontal polarization), are negligible. The averaged, normalized light scattering diagrams are shown in Fig. 5. Only one polarization (vertical) is shown because the expected changes are barely visible in the horizontal polarization diagrams. For analysis of the variation in the scattering pattern the asymmetry parameter g, which describes the relationship between the light scattered in forward and back directions, is used [34]. Its value can be calculated by the following equation:

$$g = \langle \cos\theta \rangle = \frac{1}{2}\int_{-1}^{1} d(\cos\theta) p(\theta) \cos\theta, \tag{12}$$

where $p(\theta)$ is the phase function given by

$$p(\theta) = \frac{4\pi}{C_{sca}} \frac{dC_{sca}}{d\Omega}, \tag{13}$$

where $dC_{sca}/d\Omega$ is the differential cross section and C_{sca} is the total cross section defined by the formula:

$$C_{sca} = \int_{4\pi} d\Omega \frac{dC_{sca}}{d\Omega}. \tag{14}$$

Another parameter commonly used to describe scattering properties of fractal-like aggregates is MAC (mass absorption cross section) [20], which is defined by the following equation:

$$MAC = \frac{3C_{abs}}{4\pi R_V^3 \rho} = \frac{3Q_{abs}}{4R_v \rho}, \tag{15}$$

where R_v is the volume-equivalent radius. If we assume that aggregates are composed of spherical particles in point contact, it is given by

$$R_v = r_p N_p^{(1/3)}. \tag{16}$$

However, for more complex structures (e.g. sintered or polydisperse aggregates) this equation does not apply. Many different values for the mass density ρ can be found in the literature. However, in our study we use the value proposed by Bond et al. [21] which is $\rho = 1.8\ \mathrm{g/cm}^3$. Authors also suggest that the MAC value for fresh, light-absorbing carbon is $7.5 \pm 1.2\ \mathrm{m}^2/\mathrm{g}$ and can change due to the aging process. This value is in good agreement with our measurements, although our aggregate models are not based on structures

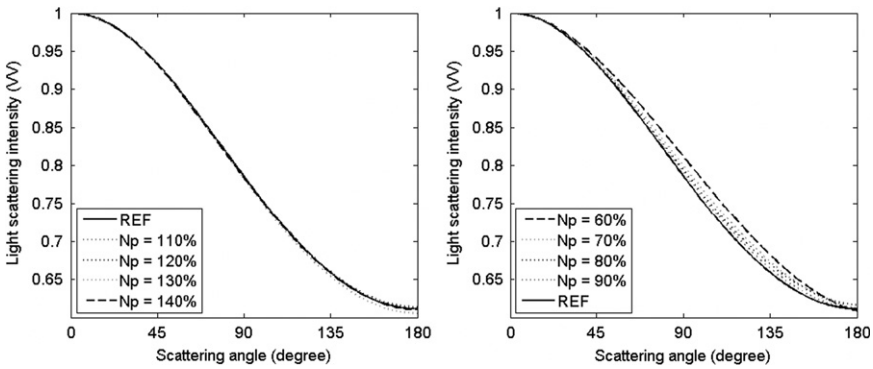

Fig. 5. The impact of the number of particles on the light scattering diagrams.

that can be encountered in the atmosphere and almost all morphological parameters differ.

With the aid of the scattering diagrams it is clearly seen that the number of particles (i.e. the total volume and surface of an aggregate) does not have a large impact on the backscattering (the asymmetry parameter varies from 0.096 to 0.100). However, it slightly changes the slope of the function regarding the intensity of scattered light. This change is better visible when the total volume is decreased (e.g. by $\sim 40\%$). The difference between the reference data and the obtained scattering diagrams as well as the resulting efficiencies for unpolarized light are presented in Table 2. One can see that both efficiencies (Q_{abs}, Q_{sca}), which are dimensionless equivalents of cross sections, increase with the number of particles. The overlap error, which slightly affects the aggregate morphology, exists only when high values of the fractal prefactor are used and the averaged error is at its maximum when the number of particles is low ($N_p=20$). Obtained results are valid only for relatively small structures. Otherwise, when larger aggregates are considered, the changes to the total volume and surface may have undeniable impact on the light scattering diagrams due to the transition from Guiner to Power Law regime [10]. Note that soot aggregates encountered in the atmosphere are usually composed of much larger number of primary particles (up to 800) [20,5]. Therefore, our study does not cover the behavior of such structures.

5.2. The impact of the radius of gyration on light scattering diagrams

Next we like to study the impact of the radius of gyration on the light scattering diagrams. For these studies six additional sets of aggregates were created. Each of them consists of 1000 different aggregates (including the reference set) composed of identical, spherical particles. Larger sets were not needed because the differences in results are significant and can be clearly seen even when small sets are used. All the parameters, except the radius of gyration R_g and the fractal prefactor k_f, are considered constant. Their values are presented in Table 3. In some cases, a small overlap error persists.

For scattering simulations we used the T-Matrix code. Every set was averaged over its size and compared to the reference data. The normalized results are presented in Fig. 6. They clearly show that the level of backscattering is dependent on the radius of gyration (the asymmetry parameter increases from 0.073 for $R_g = 42.67$ nm to 0.128 for $R_g = 57.73$ nm) what can also be seen in Table 3 in which scattering errors are listed). The total extinction ($Q_{ext} = 0.439$), scattering ($Q_{sca} = 0.010$) and absorption ($Q_{abs} = 0.430$) efficiencies for unpolarized light can be taken as constant parameters throughout all results, their variations are less than 0.003. In accordance to the general light scattering theory, if the Guinier regime is considered, the

Table 3
Impact of the radius of gyration on the light scattering diagrams. Results of the light scattering simulations and parameters of every set of aggregates. Constant parameters: $N_p=33$, $r_p = 9.94$ nm, $D_f=1.78$.

Set	1	2	3	REF	4	5	6
R_g (%)	85	90	95	100	105	110	115
R_g (nm)	42.67	45.18	47.69	50.20	52.71	55.22	57.73
k_f	2.46	2.23	2.02	1.84	1.69	1.56	1.44
C	0.010	0.006	0.002	~ 0	~ 0	~ 0	~ 0
Q_{abs}	0.431	0.432	0.431	0.430	0.429	0.429	0.429
Q_{sca}	0.010	0.010	0.010	0.010	0.010	0.009	0.009
g	0.073	0.082	0.088	0.096	0.112	0.112	0.128
MAC (m^2/g)	5.623	5.646	5.623	5.620	5.607	5.607	5.607
$E_{Avg/VV}$ (%)	6.695	4.085	2.686	–	3.029	4.917	6.810
$E_{Avg/HH}$ (%)	6.672	3.940	2.574	–	2.960	5.002	6.752

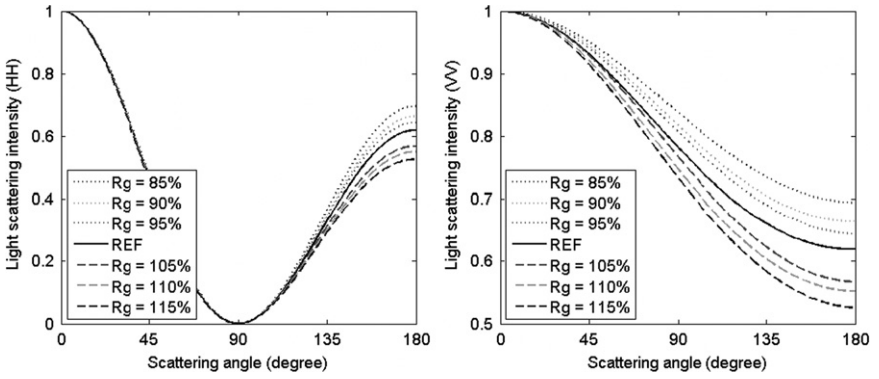

Fig. 6. The impact of the radius of gyration on the light scattering diagrams.

intensity of the scattered light can be approximated by the following equation:

$$I(q) = I(0)(1-q^2R_g^2/3), \tag{17}$$

where q is the magnitude of the scattering wave vector [10], given by

$$q = \frac{4\pi}{\lambda}\sin\left(\frac{\theta}{2}\right). \tag{18}$$

This formula is valid for $qR_g < 1$ [35,10] and clearly states that the light intensity decreases along with the increase of the radius of gyration. This effect can be seen in Fig. 6 in the light scattering pattern for VV-polarization. Aggregates, that are found in the atmosphere, can be characterized by a much larger value of the radius of gyration (which varies from $R_g = 99$ nm to $R_g = 1017$ nm) [5] and studied changes are likely to be much more significant.

5.3. The impact of the fractal dimension on light scattering diagrams

During this study we wanted to examine the impact of the fractal dimension D_f on light scattering diagrams. However, it was not possible to change its value significantly and keep the other morphological parameters unchanged (N_p, R_g and r_p). For this reason, only values which are suitable for freshly created aggregates ($D_f < 2$) were used. This is a severe limitation. According to recent research, the absorption cross section and the asymmetry parameter are almost unaffected in this region and change dramatically beyond this limit (i.e. when $D_f > 2$) [22]. Another parameter, which is responsible for the fractal behavior of soot aggregates, is the fractal prefactor k_f. According to the paper by Ehrl et al. [36] it is related to the fractal dimension and can be approximated by the following formula:

$$k_f = 4.46 \cdot D_f^{-2.08}. \tag{19}$$

However, in our study, the value of k_f is not calculated using this relation because other parameters are known and the exact solution (Eq. (1)) can be used instead. Note that values of k_f, used throughout this paper, are much larger than those which are commonly used to describe soot aggregates typically encountered in the atmosphere (the fractal prefactor varies from k_f=0.25 to k_f=1.6) [5]. However, they are out of the scope of this paper.

For these studies four sets of aggregates, composed of 5000 aggregates each, were created. When smaller quantities were used, the deviation of the scattering results by different sets (composed of the same number of elements) was significant, therefore more accurate data was needed. The fractal dimension, used in the generation of the reference data, was D_f=1.78. The variable parameters are presented in Table 4. For higher values of the fractal prefactor a small, barely noticeable, overlap error persists.

The results show that if the fractal dimension was changed, in respect to the fractal equation (by modifying also the fractal prefactor k_f), the fractal morphology as well as the scattering diagrams do not change significantly. All possible variations to the scattering parameters are suppressed by a parallel modification of k_f. The absorption efficiency ($Q_{abs} \approx 0.430$, $\Delta Q_{abs} \approx 0.001$), the scattering efficiency ($Q_{sca} \approx 0.010$, $\Delta Q_{sca} < 0.001$) and the asymmetry parameter ($g \approx 0.098$, $\Delta g \approx 0.001$) can be considered as constant throughout all results. No visible difference was found and therefore light scattering patterns are not presented in this section. Resulting errors are listed in Table 4. Note that the changes might be much more significant for larger structures characterized by higher fractal dimension.

5.4. The impact of the particle radius on light scattering diagrams

In the atmosphere the particle radius varies from $r_p = 10$ nm to $r_p = 50$ nm. The value of the median is $\sigma r =$ 22 nm [23]. However, small aggregates are often composed of particles with smaller radius [20]. In our study, the base value of the particle radius $r_p = 9.94$ nm is located at the lowest end of the above quoted range.

The morphology of aggregates, used in this study, is described in Table 5. Each set, including the reference data, is composed of 5000 elements. Like in the previous study, initial light scattering simulations (by sets composed of 1000 elements) showed that the deviation between obtained results and the reference data is relatively small and more precise results are needed.

Besides the particle radius, the total volume and the total surface of the aggregates of course also change and can be easily calculated using standard equations. Note

Table 4
Impact of the fractal dimension on the light scattering diagrams. Results of the light scattering simulations and parameters of every set of aggregates. Constant parameters: N_p=33, $R_g = 50.20$ nm, $r_p = 9.94$ nm.

Set	1	2	REF	3	4
D_f (%)	90	95	100	105	110
D_f	1.60	1.69	1.78	1.87	1.96
k_f	2.46	2.13	1.84	1.60	1.38
C	0.008	0.003	~0	~0	~0
Q_{abs}	0.429	0.430	0.430	0.430	0.430
Q_{sca}	0.010	0.010	0.010	0.010	0.010
g	0.098	0.098	0.098	0.099	0.099
MAC (m^2/g)	5.607	5.620	5.620	5.620	5.620
$E_{Avg/VV}$ (%)	0.058	0.084	–	0.111	0.175
$E_{Avg/HH}$ (%)	0.625	0.263	–	0.408	0.456

Table 5
Impact of the particle radius on the light scattering diagrams. Results of the light scattering simulations and parameters of every set of aggregates. Constant parameters: N_p=33, $R_g = 50.20$ nm, D_f=1.78.

Set	1	2	REF	3	4
r_p (%)	80	90	100	110	120
r_p (nm)	7.95	8.94	9.94	10.93	11.93
k_f	1.24	1.53	1.84	2.19	2.55
C	~0	~0	~0	0.005	0.012
Q_{abs}	0.340	0.384	0.430	0.477	0.522
Q_{sca}	0.004	0.006	0.010	0.014	0.021
g	0.099	0.099	0.098	0.100	0.099
MAC (m^2/g)	5.556	5.578	5.620	5.634	5.684
$E_{Avg/VV}$ (%)	0.799	0.367	–	0.424	0.240
$E_{Avg/HH}$ (%)	1.391	0.762	–	1.091	1.785

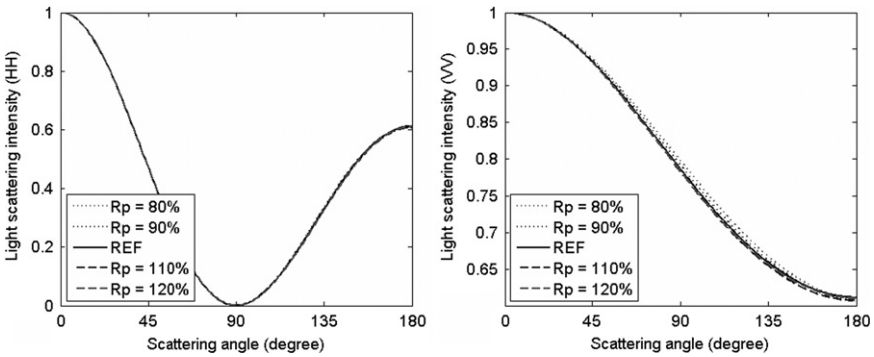

Fig. 7. The impact of the particle radius on the light scattering diagrams.

Table 6
Impact of the overlap level on the light scattering diagrams (different R_g). Results of the light scattering simulations and parameters of every set of aggregates. Constant parameters: $N_p=33$, $R_{g_0}=50.20$ nm, $r_p=9.94$ nm, $k_{f_0}=1.84$, $D_f\approx1.78$.

Set	REF	1	2	3	4	5
C	0	0.050	0.099	0.149	0.198	0.249
R_g (nm)	50.20	47.69	45.18	42.67	40.16	37.65
k_f	1.84	2.06	2.30	2.57	2.86	3.20
S_A (nm^2)	40 973	38 945	36 915	34 875	32 826	30 769
V_A (nm^3)	135 757	135 264	133 820	131 462	128 233	124 171
Q_{abs}	0.446	0.451	0.452	0.451	0.448	0.445
Q_{sca}	0.010	0.010	0.010	0.010	0.010	0.010
g	0.097	0.087	0.078	0.071	0.067	0.057
R_v (nm)	31.883	31.844	31.731	31.543	31.283	30.949
MAC (m^2/g)	5.829	5.901	5.935	5.958	5.967	5.991
$E_{Avg/VV}$ (%)	–	2.161	3.979	6.167	7.446	9.984
$E_{Avg/HH}$ (%)	–	3.342	5.302	7.550	9.444	11.764

that these parameters, in some cases, are slightly shifted from the expected values due to the overlap error. Nevertheless, the difference is rather small (less than 2%). The T-Matrix program was used and the results were averaged over all the elements included in a single set (5000 light scattering patterns). The normalized scattering diagrams are presented in Fig. 7. They show that the examined parameter has relatively small impact on the backscattering (the asymmetry parameter varies form 0.098 to 0.100). However, it slightly changes the slope in the light scattering diagram for the vertical polarization.

A similar effect can be achieved by altering the number of particles or introducing the overlap parameter. Both approaches lead to decreased volume and surface of the aggregates. Resulting parameters are presented in Table 5. One can see that the efficiencies Q_{sca}, Q_{abs} are not constant and increase along with the total volume of the aggregate. Q_{abs} is directly proportional to the particle radius $Q_{abs}/r_p\approx 0.043$. Both E_{Avg} are larger when the particle radius is far from the reference value ($r_p=9.94$ nm).

5.5. The impact of the overlap coefficient on light scattering diagrams

Next we investigate the impact of the overlap coefficient on the light scattering patterns. The first step was to create aggregates characterized by different overlap level. The radius of gyration decreases along with C, other morphology parameters are left unchanged. The desired radius of gyration R_g, the fractal prefactor k_f and other parameters are listed in Table 6. R_v, which cannot be calculated in this study by Eq. (16), is also presented. Each set consists of 1000 aggregates. Similar to the study regarding the radius of gyration, the differences in results are obvious, therefore larger sets are not needed. The total number of dipoles per wavelength ($D_w=133$) and the DDScat criterion ($|m|kd=0.079$) are constant throughout all the simulations. Due to the overlap between primary particles the DDScat code was used for scattering computations. Every set of results was averaged over its size. The normalized results for VV-scattering are presented in Fig. 8.

The changes of the radius of gyration have direct impact on the backscattering which changes the scattered intensity accordingly to Eq. (17). The other differences are more difficult to identify. The scattering efficiencies change only insignificantly ($Q_{abs}\approx0.448$, $\Delta Q_{abs}\approx0.004$, $Q_{sca}\approx0.010$, $\Delta Q_{sca}<0.001$) and the asymmetry parameter q decreases from 0.097 ($C=0$) to 0.057 ($C=0.25$). Deviations from the reference data set, presented in Table 6, increase along with the overlap level. In a second step we created five sets of aggregates characterized by different C, but the same radius of gyration R_g. All the parameters were set in accordance to following table, Table 7. For more accurate light scattering calculations, larger sets (5000 aggregates each) were created. Due to the non-zero overlap level, each aggregate was decomposed into different number of dipoles N_d. However, the

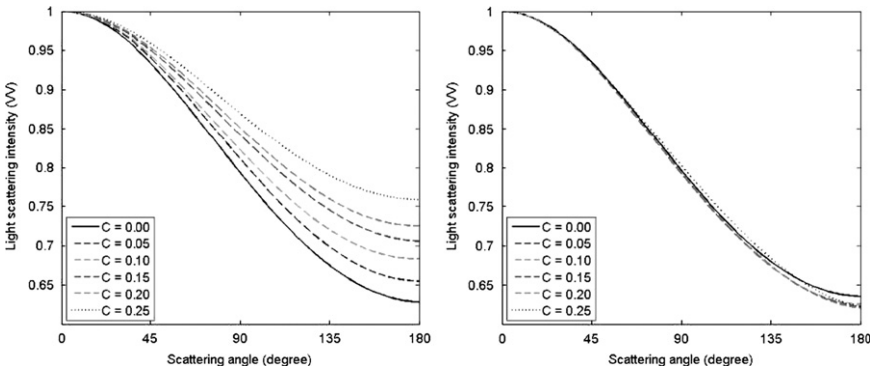

Fig. 8. The impact of the overlap level on the light scattering diagrams. Both approaches, with (left) and without (right) the changes to the radius of gyration (R_g) are presented.

Table 7
Impact of the overlap level on the light scattering diagrams (constant R_g). Results of the light scattering simulations and parameters of every set of aggregates. Constant parameters: $N_p=33$, $R_g=50.20$ nm, $r_p=9.94$ nm, $k_f=1.84$, $D_f\approx1.78$.

Set	REF	1	2	3	4	5
C	0	0.05	0.10	0.15	0.20	0.25
R_{g_0} (nm)	50.20	53.68	56.66	59.99	63.75	67.99
k_{f_0}	1.84	1.61	1.44	1.29	1.16	1.04
S_A (nm^2)	40 973	38 986	36 999	35 013	33 026	30 726
V_A (nm^3)	135 757	135 271	133 848	131 536	128 384	124 083
Q_{abs}	0.447	0.450	0.451	0.450	0.447	0.443
Q_{sca}	0.010	0.010	0.010	0.010	0.010	0.009
g	0.094	0.096	0.097	0.098	0.100	0.099
R_v (nm)	31.883	31.845	31.733	31.549	31.295	30.942
MAC (m^2/g)	5.842	5.888	5.922	5.943	5.951	5.966
$E_{Avg/VV}$ (%)	–	0.572	0.662	0.621	0.617	0.515
$E_{Avg/HH}$ (%)	–	1.736	2.292	2.749	3.110	3.772

number of dipoles per wavelength ($D_w=133$) and the DDScat criterion ($|m|kd=0.079$) were kept constant.

The diagram for vertical polarization is in good agreement with the reference data. Small differences exist, but they are quite random. They could be caused by the lack of changes to the fractal dimension D_f in our aggregate model (only k_f and R_g were adjusted according to Eqs. (10) and (11)). Nevertheless, if we introduce the overlap parameter and keep the mentioned equations satisfied, the scattering diagrams will not change significantly. The scattering efficiencies can be considered as constants ($Q_{abs}\approx0.447$, $\Delta Q_{abs}\approx0.004$, $Q_{sca}\approx0.010$, $\Delta Q_{sca}\approx0.001$). The asymmetry parameter varies from 0.094 to 0.100. The scattering errors similarly increase with the overlap level. However, this time the changes are relatively small and can be neglected. This suggests that an aggregate composed of overlapping spheres can be replaced by an aggregate that consist of particles being in point contact.

5.6. The impact of the laser wavelength on light scattering diagrams

The laser wavelength is usually a fixed parameter, dependent on the used experimental set-up, and cannot be changed easily. Its influence on the light scattering diagrams is strictly coupled with the size of the structure. This study is similar to changing both the radius of gyration R_g and the particle size r_p simultaneously. However, this time the resulting error is less significant, because there is no need for changing the morphological parameters of aggregates. For these studies only one set composed of 1000 aggregates was created, but simulations, performed with the T-Matrix program, were repeated four times, each time with a different incident wavelength (Table 8). Because of the lack of changes to the morphological parameters, larger sets were not needed.

Table 8
Impact of the laser wavelength on the light scattering diagrams. Results of the light scattering simulations and parameters of every set of aggregates. Constant parameters: $N_p=33$, $R_g=50.20$ nm, $r_p=9.94$ nm, $k_f=1.84$, $D_f=1.78$.

Set	1	2	REF	3	4
λ (%)	80	90	100	110	120
λ (nm)	426.6	478.8	532.0	585.2	638.4
Q_{abs}	0.540	0.480	0.430	0.389	0.356
Q_{sca}	0.021	0.014	0.010	0.007	0.005
g	0.151	0.120	0.098	0.081	0.068
MAC (m^2/g)	7.057	6.273	5.620	5.084	4.624
$E_{Avg/VV}$ (%)	11.860	5.076	–	4.774	8.279
$E_{Avg/HH}$ (%)	11.531	4.975	–	4.636	8.047

The results (Fig. 9) show that the changes are highly visible and affect mostly backscattering (the asymmetry parameter varies from 0.151 for $\lambda=426.6$ nm to 0.068 for $\lambda=638.4$ nm). The laser wavelength is a well-known,

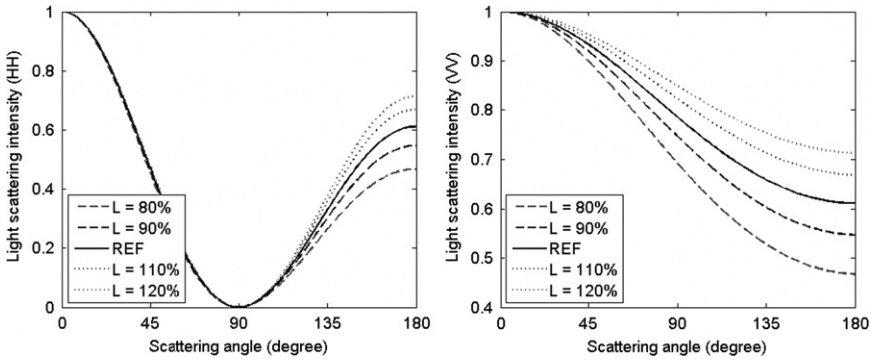

Fig. 9. The impact of the laser wavelength on the light scattering diagrams.

Table 9
Impact of the refractive index on the light scattering diagrams. Results of the light scattering simulations and parameters of every set of aggregates. Constant parameters: N_p=33, R_g = 50.20 nm, r_p = 9.94 nm, k_f=1.84, D_f=1.78.

Set	Re 1	Re 2	Re 3	Re 4
m	70%+100%i	85%+100%i	115%+100%i	130%+100%i
m	1.099+0.560i	1.335+0.560i	1.806+0.560i	2.041+0.560i
Q_{abs}	0.549	0.489	0.376	0.328
Q_{sca}	0.006	0.007	0.013	0.017
g	0.098	0.098	0.097	0.097
MAC (m^2/g)	7.175	6.391	4.914	4.287
$E_{Avg/VV}$ (%)	0.456	0.489	0.572	0.593
$E_{Avg/HH}$ (%)	1.207	0.912	1.385	2.461
Set	Im 1	Im 2	Im 3	Im 4
m	100%+70%i	100%+85%i	100%+115%i	100%+130%i
m	1.570+0.392i	1.570+0.476i	1.570+0.644i	1.570+0.728i
Q_{abs}	0.305	0.369	0.492	0.552
Q_{sca}	0.007	0.008	0.011	0.013
g	0.097	0.097	0.097	0.097
MAC (m^2/g)	3.986	4.822	6.430	7.214
$E_{Avg/VV}$ (%)	0.539	0.531	0.520	0.515
$E_{Avg/HH}$ (%)	0.920	0.690	0.839	1.311
Set	M 1	M 2	M 3	M 4
m	70%+70%i	85%+85%i	115%+115%i	130%+130%i
m	1.099+0.392i	1.335+0.476i	1.806+0.644i	2.041+0.728i
Q_{abs}	0.382	0.416	0.429	0.419
Q_{sca}	0.003	0.006	0.015	0.020
g	0.097	0.097	0.097	0.097
MAC (m^2/g)	4.992	5.437	5.607	5.476
$E_{Avg/VV}$ (%)	0.483	0.499	0.558	0.592
$E_{Avg/HH}$ (%)	1.891	1.240	1.740	3.158

constant parameter and can be determined before measurements. The results show that the scattering diagrams can be easily adjusted and compared to other diagrams, obtained with the use of different laser wavelengths. This relationship could be useful when several experimental set-ups are used. However, this simplification could be used only with the light scattering diagrams because of the sharp changes in the other parameters, presented in Table 8.

5.7. The impact of the refractive index on light scattering diagrams

There is much uncertainty within the literature to what extent the refractive index m of soot may be approximated by a constant, i.e. independent of wavelength within a range relevant for light scattering investigations and the conditions of soot formation, e.g. type of fuel or equivalence ratio. Strictly speaking, a variation is of course to be expect. One common value in the literature is $m = 1.57 + 0.56i$ [37] though the authors underline that this value has never been derived experimentally. A list of other values, commonly used for soot aggregates encountered in the atmosphere, can be found in the review by Bond et al. [21]. For studies regarding the impact of the refractive index the same set, as during the previous studies (composed of 1000 aggregate structures), was used. The simulations were performed 12 times (Table 9). The huge spread of the values (both the real and the imaginary parts) was used to cover many

possible variations of this parameter. Additionally, alternative values are also discussed (e.g. $m=1.60+0.60i$, $m=1.57+0.48i$ [37], $m=2.10+0.48i$ [38]).

The changes in the scattering diagrams for vertical polarization are barely visible. Therefore, only errors, instead of diagrams, are presented (Tables 9 and 10). They are relatively small and even huge changes to the refractive index do not have meaningful impact on the light scattering diagrams, as long as we only consider normalized data. Of course, absolute light scattering intensities change drastically. The level of backscattering can be considered as constant (the asymmetry parameter changes slightly from 0.097 to 0.098) what is in good agreement with the study by Kahnert [39] who concludes that g is rather insensitive to variations of the refractive index m. Therefore, we conclude that, if only normalized light scattering diagrams are considered, all the alterations of the refractive index, caused by the experimental set-up or environmental conditions, can be neglected. This conclusion is only valid for small soot aggregates generated under laboratory conditions, which are described in this paper (17 mm HAB, $\phi=2.5$). As expected, large differences were observed in the efficiencies Q_{sca}, Q_{abs} (Table 11).

6. Concluding discussion

In our study we investigated the impact of the variation of various parameters of fractal aggregates, which can be found under laboratory conditions, on light scattering patterns. Generated aggregates were much smaller ($R_g \approx 50.20$ nm) than those, which are usually encountered in the atmosphere [23]. Our results are not relevant for atmospheric optics and therefore, might be of limited interest to climate scientists.

The study demonstrates that the most influential factor on the scattering pattern of soot aggregates, among all the fractal equation parameters, is the radius of gyration R_g. Its impact on the light scattering diagrams can be seen in Figs. 6 and 8. Even a small change of its value leads to significant changes in the amount of light scattered towards the back direction. The fractal dimension D_f and the fractal prefactor k_f are responsible for fractal-like behavior of aggregates. If we alter both of them in a way that the fractal equation is satisfied (Table 4), no changes in the scattering diagrams would be visible. However, we were able to create aggregates with the fractal dimension up to $D_f=1.96$. This severe limitation was caused by the aggregation code and could not be omitted. All the procedures that lead to the change of the total volume V_A and the total surface S_A of an aggregate (e.g. modifications of r_p or N_p) can affect the shape of the resulting scattering diagrams. Nonetheless, backscattering stays almost unaffected (Figs. 5 and 7). The overlap factor C introduces barely visible changes to the results, but only if the radius of gyration is kept constant (Fig. 8). Changes to the incident wavelength λ have impact on the amount of light scattered in back direction (Fig. 9) and the refractive index m introduces only barely visible changes to the normalized scattering patterns (Table 9). However, the efficiencies (Q_{abs}, Q_{sca}) are highly affected. Surprisingly, averaging over a set of scattering diagrams which contains 1000 elements is not sufficient to ade-

Table 10
Impact of various refractive indices on the light scattering diagrams. Constant parameters: $N_p=33$, $R_g=50.20$ nm, $r_p=9.94$ nm, $k_f=1.84$, $D_f=1.78$.

Set	REF	1	2	3
m	1.57+0.56i	1.60+0.60i	1.57+0.48i	2.10+0.48i
Q_{abs}	0.430	0.452	0.370	0.273
Q_{sca}	0.010	0.011	0.009	0.017
g	0.096	0.097	0.097	0.097
MAC (m^2/g)	5.62	5.907	4.835	3.568
$E_{Avg/VV}$ (%)	–	0.409	0.429	0.541
$E_{Avg/HH}$ (%)	–	0.743	0.689	2.544

Table 12
Required number of aggregates in relation to simulation studies of every discussed parameter.

Parameter	Number of aggregates
N_p	5000
R_g	1000
D_f	5000
r_p	5000
λ	1000
m	1000
C, different R_g	1000
C, constant R_g	1000

Table 11
Impact of various refractive indices commonly used for atmospheric soot aggregates [21] on the light scattering diagrams. Constant parameters: $N_p=33$, $R_g=50.20$ nm, $r_p=9.94$ nm, $k_f=1.84$, $D_f=1.78$.

Set	1	2	3	4	5
m	1.75+0.63i	1.80+0.67i	1.85+0.71i	1.90+0.75i	1.95+0.79i
Q_{abs}	0.434	0.447	0.458	0.468	0.477
Q_{sca}	0.014	0.015	0.016	0.019	0.019
g	0.097	0.097	0.097	0.097	0.097
MAC (m^2/g)	5.672	5.842	5.985	6.116	6.234
$E_{Avg/VV}$ (%)	0.561	0.588	0.812	0.479	0.492
$E_{Avg/HH}$ (%)	0.877	1.328	2.199	2.684	3.109

quately simulate light scattering in most instances. This size can be only used when changes of the scattered intensities are significant (e.g. while changing the radius of gyration Fig. 6) or if the morphological parameters stay unchanged throughout all the simulations (e.g. while changing the incident wavelength Fig. 9). Otherwise, more accurate results are needed to distinguish the desired phenomenon from a noise, which is caused by the averaging of insufficient number of scattering patterns. The number of aggregates used in the simulation studies is presented in Table 12. Our study is based on data that were experimentally observed in a typical light-scattering experiment. One must be aware, however, that also experimental situations may arise where soot aggregates with quite different characteristics may be found, e.g., much larger aggregates (with the diameter as large as 1000 nm [23]) which are commonly encountered in the atmosphere. Nonetheless the investigations performed are helpful to identify the parameters that must be given special consideration in experiments. For example, we have shown that the overlap parameter is not critical as compared to the radius of gyration. One practical consequence is that an exact determination of the overlap parameter from TEM data is dispensable, or vice versa, that a determination of this parameter from light scattering experiments is hardly possible.

The procedure for obtaining morphological parameters of fractal aggregates that give light scattering results close to measurement data is promising (Section 4). It suggests that it is possible to replace a size distribution of aggregate sizes by a characteristic average value. Nonetheless further studies are certainly required that address the issue of distributions (of primary particle sizes or the number of primary particles per aggregate). For further computational studies the small effect of the overlap factor opens promising perspectives: it might be possible to omit this what would significantly decrease computation time (the T-Matrix code could be used instead of the slower DDScat program, Fig. 8).

Acknowledgments

We would like to acknowledge support of this research by the Deutsche Forschungsgemeinschaft (DFG).

References

[1] Brasil AM, Farias TL, Carvalho G. A recipe for image characterization of fractal-like aggregates. J Aerosol Sci 1999;30:1379–89.
[2] Wozniak M, Onofri FRA, Barbosa S, Yon J, Mroczka J. Comparison of methods to derive morphological parameters of multi-fractal samples of particle aggregates from tem images. J Aerosol Sci 2012;47:12–26.
[3] Dobbins R, Megaridis C. Morphology of flame-generated soot as determined by thermophoretic sampling. Langmuir 1987;3:254–9.
[4] Koylu UO, Xing Y, Rosner D. Fractal morphology analysis of combustion-generated aggregates using angular light scattering and electron microscope images. Langmuir 1995;11:4848–54.
[5] Adachi K, Chung SH, Friedrich H, Buseck PR. Fractal parameters of individual soot particles determined using electron tomography: implications for optical properties. J Geophys Res 2007;112:D14202. http://dx.doi.org/10.1029/2006JD008296.
[6] Poppel LL, Friedrich H, Spinsby J, Chung SH, Seinfeld JH, Buseck PR. Electron tomography of nanoparticle clusters: implications for atmospheric lifetimes and radiative forcing of soot. Geophys Res Lett 2005;32:L24811. http://dx.doi.org/10.1029/2005GL024461.
[7] Will S, Schraml S, Bader K, Leipertz A. Performance characteristics of soot primary particle size measurements by time-resolved laser-induced incandescence. Appl Opt 1998;37:5647–58.
[8] Iuliis SD, Cignoli F, Zizak G. Two-color laser-induced incandescence (2C-LII) technique for absolute soot volume fraction measurements in flames. Appl Opt 2005;44:7–8.
[9] Ryser R, Gerber T, Dreier T. Soot particle sizing during high-pressure diesel spray combustion via time-resolved laser-induced incandescence. Combust Flame 2009;156:120–9.
[10] Sorensen CM. Light scattering by fractal aggregates: a review. Aerosol Sci Technol 2001;35:648–87.
[11] Oltmann H, Reimann J, Will S. Single-shot measurement of soot aggregate sizes by wide-angle light scattering (WALS). Appl Phys B: Lasers Opt 2012;106:171–83.
[12] Oltmann H, Reimann J, Will S. Wide-angle light scattering (WALS) for soot aggregates characterization. Combust Flame 2010;157:516–22.
[13] Waterman PC. Symmetry, unitarity and geometry in electromagnetic scattering. Phys Rev D 1971;3:825–39.
[14] DeVoe H. Optical properties of molecular aggregates i. classical model of electronic absorption and refraction. J Chem Phys 1964;41:393–400.
[15] DeVoe H. Optical properties of molecular aggregates i. classical theory of the refraction, absorption, and optical activity of solutions and crystals. J Chem Phys 1965;43:3199–208.
[16] Purcell EM, Pennypacker CR. Scattering and absorption of light by nonspherical dielectric grains. Astrophys J 1973;186:707–14.
[17] Doicu A, Wriedt T. T-matrix method for electromagnetic scattering from scatterers with complex structure. J Quant Spectrosc Radiat Transfer 2001;70:663–73.
[18] Draine BT, Flatau PJ. Discrete-dipole approximation for scattering calculations. J Opt Soc Am A 1994;4:1491–9.
[19] Weitz DA, Oliviera M. Fractal structures formed by kinetic aggregation of aqueous gold colloids. Phys Rev Lett 1984;52:1433–6.
[20] Kahnert M, Devasthale A. Black carbon fractal morphology and short-wave radiative impact: a modelling study. Atmos Chem Phys 2011;11:11745–59.
[21] Bond TC, Bergstrom RW. Light absorption by carbonaceous particles: an investigative review. Aerosol Sci Technol 2006;40:27–67.
[22] Liu L, Mishchenko MI, Arnott WP. A study of radiative properties of fractal soot aggregates using the superposition t-matrix method. J Quant Spectrosc Radiat Transfer 2008;109:2656–63.
[23] Adachi K, Buseck PR. Internally mixed soot, sulfates, and organic matter in aerosol particles from Mexico city. Atmos Chem Phys 2008;8:6469–81.
[24] Cai J, Lu N, Sorensen CM. Analysis of fractal cluster morphology parameters: structural coefficient and density autocorrelation function cutoff. J Colloid Interface Sci 1995;470–473:171.
[25] Filippov A, Zurita M, Rosner D. Fractal-like aggregates: relation between morphology and physical properties. J Colloid Interface Sci 2000;229:261–73.
[26] Oh C, Sorensen CM. The effect of overlap between monomers on the determination of fractal cluster morphology. J Colloid Interface Sci 1997;193:17–25.
[27] Brasil AM, Farias TL, Carvalho G, Koylu UO. Numerical characterization of the morphology of aggregated particles. J Aerosol Sci 2001;32:489–508.
[28] Meakin P. A historical introduction to computer models for fractal aggregates. J Sol–Gel Sci Technol 1999;15:97–117.
[29] Mroczka J, Wozniak M, Onofri FRA. Algorithms and methods for analysis of the optical structure factor of fractal aggregates. Metrol Meas Syst 2012;19:459–70.
[30] Penttila A, Zubko E, Lumme K, Muinonen K, Yurkin M, Draine B, et al. Comparison between discrete dipole implementations and exact techniques. J Quant Spectrosc Radiat Transfer 2007;106:417–36.
[31] Comberg U, Wriedt T. Comparison of scattering calculations for aggregated particles based on different models. J Quant Spectrosc Radiat Transfer 1999;63:149–62.
[32] Schmid HJ, Tejwani S, Artelt C, Peukert W. Monte Carlo simulation of aggregate morphology for simultaneous coagulation and sintering. J Nanoparticle Res 2004;6:613–26.
[33] Riefler N, Stasio S, Wriedt T. Structural analysis of clusters using configurational and orientational averaging in light scattering analysis. J Quant Spectrosc Radiat Transfer 2004;89:323–42.

[34] Mishchenko MI. Asymmetry parameters of the phase function for densely packed scattering grains. J Quant Spectrosc Radiat Transfer 1994;52:95–110.
[35] Sorensen CM, Lu N, Cai J. Fractal cluster distribution measurement using static light scattering. J Colloid Interface Sci 1995;174:456–60.
[36] Ehrl L, Soos M, Lattuada M. Generation and geometrical analysis of dense clusters with variable fractal dimension. J Phys Chem B 2009;113:10587–99.
[37] Smyth K, Shaddix C. The elusive history of m = 1.57–0.56i for the refractive index of soot. Combust Flame 1996;107:314–20.
[38] Van-Hulle P, Talbaut M, Weill M, Coppalle A. Inversion method and experiment to determine the soot refractive index: application to turbulent diffusion flames. Meas Sci Technol 2002;13:375–82.
[39] Kahnert M. On the discrepancy between modeled and measured mass absorption cross sections of light absorbing carbon aerosols. Aerosol Sci Technol 2010;44:453–60.